

# UV slopes of Starforming Galaxies in Strong Lensing fields at the Epoch of Reionization with JWST

Giordano Felicioni<sup>1</sup> , Maruša Bradač<sup>1,2</sup> , Yoshihisa Asada<sup>3</sup> , Nicholas S. Martis<sup>1</sup> , Ghassan T. E. Sarrouh<sup>4</sup> , Guillaume Desprez<sup>5</sup> , Gregor Rihtaršič<sup>1</sup> , Naadiyah Jagga<sup>4</sup> , Anishya Harshan<sup>6,7</sup> , Jon Judež<sup>1</sup> , Chris J. Willott<sup>8</sup> , Roberto Abraham<sup>3,9</sup> , Gabriel Brammer<sup>10,11</sup> , Vince Estrada-Carpenter<sup>12,13</sup> , Jasleen Matharu<sup>14</sup> , Adam Muzzin<sup>15</sup>, Gaël Noiro<sup>16</sup>, Marcin Sawicki<sup>17</sup> , Sunna Withers<sup>15</sup> , Vladan Markov<sup>1</sup> , Rosa M. Mérida<sup>17</sup> , Vesna Pirc Jevšenak<sup>1</sup> , and Roberta Tripodi<sup>18</sup> 

<sup>1</sup> University of Ljubljana, Faculty of Mathematics and Physics, Jadranska ulica 19, SI-1000 Ljubljana, Slovenia

<sup>2</sup> Department of Physics and Astronomy, University of California Davis, 1 Shields Avenue, Davis, CA 95616, USA

<sup>3</sup> Dunlap Institute for Astronomy and Astrophysics, 50 St. George Street, Toronto, Ontario, M5S 3H4, Canada

<sup>4</sup> Department of Physics and Astronomy, York University, 4700 Keele St. Toronto, Ontario, M3J 1P3, Canada

<sup>5</sup> Kapteyn Astronomical Institute, University of Groningen, P.O. Box 800, 9700AV Groningen, The Netherlands

<sup>6</sup> Kavli Institute for Cosmology, University of Cambridge, Madingley Road, Cambridge, CB3 0HA, United Kingdom

<sup>7</sup> Cavendish Laboratory - Astrophysics Group, University of Cambridge, 19 JJ Thomson Avenue, Cambridge, CB3 0HE, UK

<sup>8</sup> National Research Council of Canada, Herzberg Astronomy & Astrophysics Research Centre, 5071 West Saanich Road, Victoria, BC, V9E 2E7, Canada

<sup>9</sup> David A. Dunlap Department of Astronomy and Astrophysics, University of Toronto, 50 St. George Street, Toronto, Ontario, M5S 3H4, Canada

<sup>10</sup> Cosmic Dawn Center (DAWN), Denmark

<sup>11</sup> Niels Bohr Institute, University of Copenhagen, Jagtvej 128, DK-2200 Copenhagen N, Denmark

<sup>12</sup> School of Earth and Space Exploration, Arizona State University, Tempe, AZ 85287, USA

<sup>13</sup> Beus Center for Cosmic Foundations, Arizona State University, Tempe, AZ 85287, USA

<sup>14</sup> Max-Planck-Institut für Astronomie, Königstuhl 17, D-69117 Heidelberg, Germany

<sup>15</sup> Department of Physics and Astronomy, York University, 4700 Keele St. Toronto, Ontario, M3J 1P3, Canada

<sup>16</sup> Space Telescope Science Institute, 3700 San Martin Drive, Baltimore, Maryland 21218, USA

<sup>17</sup> Department of Astronomy and Physics and Institute for Computational Astrophysics, Saint Mary's University, 923 Robie Street, Halifax, Nova Scotia B3H 3C3, Canada

<sup>18</sup> INAF - Osservatorio Astronomico di Roma, Via Frascati 33, Monte Porzio Catone, 00078, Italy

February 20, 2026

## ABSTRACT

**Context.** UV slopes ( $\beta$ ) are a powerful diagnostics for galaxies at the epoch of reionization, tracing star formation, ISM ionization, and the escape fraction  $f_{esc}$  of ionizing photons. Studies at low and intermediate  $z$  find suggest a gradual reddening of the UV slope with time and steeper slopes for fainter galaxies. With the James Webb Space Telescope (JWST), it has been possible to measure the UV slope for statistically significant samples of galaxies deep into the EoR, up to redshift  $z \gtrsim 10$  and for increasingly faint galaxies. Recent studies of  $\beta$  with JWST at  $z > 7$  reveal a flattening of the trend of the UV slope with respect to redshift and UV magnitude.

**Aims.** We want to measure  $\beta$  at  $z > 7.5$  using the strong lensing around massive galaxy clusters to observe high-redshift and faint galaxies. The low-brightness regime is of particular interest for reionization, as most of the recent models of this process posit that numerous faint galaxies are the prime drivers of reionization

**Methods.** We use NIRCam and NIRSpec observations from CANUCS, Technicolor, JUMPS, Silver Bullet, UNCOVER and MEGA-SCIENCE across 7 strong lensing fields in order to find galaxies down to  $M_{UV} \sim -16$  and  $7.5 < z \lesssim 12.5$ . We measure their  $\beta$  with a forward-modelling procedure. We estimate the  $f_{esc}$  of a subsample with emission line data using a relation with UV slope, galaxy size and  $H\beta$  equivalent width (EW $H\beta$ ) calibrated from a low-redshift sample.

**Results.** We find 378 visually confirmed galaxies, including 45 with a spectrum. We obtain an average UV slope  $\langle \beta \rangle = -2.3 \pm 0.4$ , an average redshift  $\langle z \rangle = 8.5 \pm 1.0$ , and an average AB magnitude  $M_{UV} = -18 \pm 1$ . We find no significant evolution of  $\beta$  across our redshift range, suggesting a flattening of the  $\beta - z$  trend above  $z \sim 7.5$ . We find a weak trend between  $\beta$  and  $M_{UV}$ . For a subsample of 14 galaxies with emission line data we estimate an average  $f_{esc} = 0.26 \pm 0.22$

**Conclusions.** The flat trend of  $\beta$  at  $z > 7.5$  indicates a similarity in average galaxy properties between 300 and 600 Myr after the Big Bang. The weak trend between  $\beta$  and  $M_{UV}$  suggests an analogous composition for low- and high-mass galaxies' ISM, likely due to a lack of time to build up a dust reservoir. The average  $f_{esc}$  is high for what is necessary to achieve an ionized IGM by  $z \sim 6$ , but the extrapolation model from a low-redshift sample may be overestimating its value.

**Key words.** Methods: statistical – Galaxies: high-redshift – dark ages, reionization, first stars – Ultraviolet: galaxies

## 1. Introduction

The UV continuum emission redwards of Lyman- $\alpha$  in galaxies is a powerful diagnostic of different physical properties of a galaxy. It is affected by the direct emission of stars, stellar ages and metallicities, as well as by the nebular emission of gas and reprocessing from the dust content. It is characterized as a power-law  $F_\lambda \sim \lambda^\beta$ , where  $F_\lambda$  is the wavelength-specific flux density and  $\beta$  is the characteristic index of the slope. This quantity provides insights on the stellar populations in a galaxy and on its gas and dust content (Calzetti et al. 1994). Steeper UV slopes (lower  $\beta$ ) have been associated with a higher number of young bright stars and a higher proportion of ionizing photon emission; meanwhile, heated nebular gas emits light towards longer wavelengths, tending to soften the overall UV slope.

Early studies on the evolution of the UV slope were conducted using data from the Hubble Space Telescope (HST), investigating the relationship between  $\beta_{UV}$  and other physical properties. Bouwens et al. (2010) and Bouwens et al. (2014) measured the slopes of over 4000 galaxies at  $4 < z < 8$ , finding that galaxies at earlier cosmic times have on average steeper UV slopes, suggesting that as star formation goes on, the dust reservoir builds up, softening the overall UV radiation. They also find that fainter galaxies are bluer on average, which can be read as fainter galaxies showing less attenuation in the UV in the investigated redshift range. Meanwhile, Bolamperti et al. (2023) used HST data to study individual clumps, finding that clumps also follow the same negative  $\beta - z$  and  $\beta - M_{UV}$  relations. In addition, these individual clumps show bluer slopes than that of their host galaxy as a whole.

Since the launch of the James Webb Space Telescope (JWST), it has been possible to measure the UV slope for statistically significant samples of galaxies at redshift  $z \gtrsim 10$  with individual galaxies reaching  $z_{phot} \sim 15$  in the latest studies (e.g. Asada et al. 2025), and high-redshift galaxy candidates up to  $z \sim 25$  (Pérez-González et al. 2025; Whitler et al. 2025). New data from observation programs in the first years of JWST allowed to extend these studies well into the Epoch of Reionization (EoR). The Cosmic Evolution Early Release Science Survey (CEERS, Finkelstein et al. 2023), JWST Advanced Deep Extragalactic Survey (JADES, Eisenstein et al. 2023), Prime Extragalactic Areas for Reionization Science (PEARLS, Windhorst et al. 2023), Grism Lens-Amplified Survey from Space (GLASS, Treu et al. 2022, the Next Generation Deep Extragalactic Exploratory Public (NGDEEP) survey (Bagley et al. 2024), and Ultradeep NIRSpec and NIRCam ObserVations before the Epoch of Reionization (UNCOVER, (Bezanson et al. 2024)) are only some of the first surveys that keep providing data for studies at the epoch of reionization. Several of these studies confirm the trend of fainter galaxies having bluer slopes: (Topping et al. 2023) with JADES photometric observations, (Cullen et al. 2024) with a wide sample of photometric data including GLASS, CEERS, JADES, NGDEEP and UNCOVER, (Austin et al. 2024) with photometry from the EPOCHS photometric sample, and (Dottorini et al. 2024) with spectroscopy from CEERS and JADES. They similarly find steeper UV slopes at increasing redshifts for galaxies of similar brightness. In contrast, Saxena et al. (2024), using spectral data from JADES and JADES Origin Field (JOF), find increasing reddening in galaxies at  $z > 9.5$  and a flattening of the  $\beta - M_{UV}$  trend in galaxies at  $z \gtrsim 8$ .

The UV slope proves to be a powerful diagnostic for reionization, and it's been proposed as an indicator for high escape fraction ( $f_{esc}$ ) of Lyman-Continuum photons (LyC) (Zackrisson

et al. 2013; Chisholm et al. 2022; Flury et al. 2022; Choustikov et al. 2024). Several recent studies with JWST observations have found evidence of galaxies with extremely blue UV slopes with  $\beta < -2.6$  (e.g. Topping et al. 2023; Cullen et al. 2024; Saxena et al. 2024; Austin et al. 2024): a condition which is believed to indicate the leakage of LyC radiation (e.g. Topping et al. 2023). At low redshift, where direct measurements of  $f_{esc}$  are possible, it is possible to find the relationship between the two. The HST Low-redshift Lyman-Continuum Survey (LzLCS) (Flury et al. 2022) provides a good testing ground for this. Chisholm et al. (2022) find an inverse correlation between  $\beta_{UV}$  and  $f_{esc}$ , and apply it to high-redshift galaxies to find their escape fraction, while Flury et al. (2022) also discover that a combination of diagnostics, including  $\beta$ ,  $[OIII]/[OII]$  ratio O32, and the equivalent width of the  $H\beta$  line  $EW(H\beta)$ , are better indicators of strong LyC leakage. Mascia et al. (2023, 2024) conclude that  $\beta$  slopes by themselves are not a reliable estimator, finding a relationship between measured  $f_{esc}$  and diagnostics available at high-redshift, including  $\beta$ , galaxy half-light radius  $r_e$ , and emission line diagnostics. They apply the correlation found in order to estimate  $f_{esc}$  for a sample of  $4.5 \leq z \leq 8$  galaxies with available spectroscopy.

All of the mentioned JWST studies are affected by the fact that they rely on either purely spectroscopic observations of individual high-redshift galaxies, limiting the statistics to galaxies selected for observation, or on a wide sample of NIRCam photometric observations leveraging mostly broad-band filters and only a few medium-band filters, limiting the accuracy of the measurement of  $\beta$ .

Strongly lensed cluster fields offer a great opportunity for probing the universe at high redshift, as the magnification from these fields would allow us to detect fainter luminosity galaxies, which are believed to be the source of the majority of ionizing photons for reionization. Several of these fields have already been probed by JWST surveys. Among those, the Canadian NIRISS Unbiased Cluster Survey (CANUCS) (Willott et al. 2022; Sarrouh et al. 2026) has observed with JWST's instruments NIRCam, NIR-Spec, and NIRISS, galaxies in 5 different lensed fields, allowing us to observe galaxies at very high redshifts (up to  $z \sim 13$ ). This survey has been subsequently integrated with Technicolor (PI: Muzzin) and JUMPS (co-PIs: Withers, Muzzin), two follow-up surveys which target 3 of the 5 CANUCS fields: Abell 370, MACS0416 and MACS1149. Other surveys probing strongly lensed field are *Silver Bullet for Dark Matter* (PIs Bradač, Ríhtarščík, Ríhtarščík et al. 2026), targeting the Bullet Cluster field, and UNCOVER, targeting Abell 2744 Bezanson et al. (2024); Suess et al. (2024).

This paper is organized as follows: in section 2 we present the data used for this work; in section 3 we show the procedure for selecting a reliable high-redshift sample and explain the methodology for measuring the UV slopes. We present our results in section 4, and we estimate the LyC escape fraction for a subset of our sample. We analyze the results and the evolution of  $\beta$  with redshift and with UV magnitude in section 5. Finally, we sum up our conclusions in section 6. Throughout the paper we assume a  $\Lambda$ CDM cosmology with the latest results from Planck (Aghanim et al. 2020).

## 2. Data

CANUCS - Technicolor - JUMPS CANUCS is a JWST Cycle 1 GTO galaxy survey (PID: 1208; PI: Willott; Willott et al. 2022) targeting five galaxy cluster fields: Abell 370, MACS0417, MACS0416, MACS1423, and MACS1149. A massive galaxy

cluster at the primary pointing of each cluster field causes the objects behind it to be strongly lensed and magnified. The central region (CLU pointing) of each field has been observed with NIRCam (in the Imaging mode) and NIRISS (Imaging and Wide Field Slitless Spectroscopy) instruments, and two flanking fields exist for each field: one observed with NIRISS while NIRCam was being pointed at the central CLU pointing, NSF (NIRISS Flanking field); and one targeted with NIRCam while NIRISS was pointed at the cluster, NCF (NIRCam Flanking field). Subsequent observations from *JWST* in *Technicolor* Cycle 2 program (PID: 3362; PI: Muzzin) and *JWST* Ultimate Medium-band Photometric Survey (JUMPS) Cycle 3 program (PID: 5890 co-PIs: Withers, Muzzin) add medium-band filters for respectively the NCF and the CLU pointings of the Abell 370, MACS0416 and MACS1149 fields. *Technicolor* completes the full-suit of medium- and broad-band NIRCam filters for the NCF pointing, while JUMPS adds observations in the F360M, F430M, F460M and F480M NIRCam filters for the CLU pointing. Follow-up NIRSpec Prism observations with the Micro-shutter Assembly (MSA) were carried out for selected objects in the CLU fields. These objects were selected for individual science cases by the CANUCS team (see also [Sarrouh et al. 2026](#), §2.3).

**Bullet Cluster** We also include data Bullet Cluster data taken with NIRCam in Imaging mode and with NIRSpec MOS, observed as part of the GO Program *Silver Bullet for Dark Matter* (PID: 4598; co-PIs: Bradač, Rihtaršič, Sawicki). NIRCam filters included for this field are F090W, F115W, F150W, F200W, F277W, F356W, F410M and F444W.

**GLASS - UNCOVER - MEGASCIENCE** Finally, we include NIRCam broad- and medium-band observation of the Abell 2744 cluster field from GLASS-JWST-ERS (PID: 1324 PI: Tommaso Treu [Treu et al. 2022](#), and PID: 2756 PI: Wenlai Chen), UNCOVER (PID: 2561; PIs: Ivo Labbe and Rachel Bezanson [Bezanson et al. 2024](#)), and MEGASCIENCE (PID: 4111; PI: Wren Suess [Suess et al. 2024](#)). NIRCam filters covered by the survey are F070W, F090W, F115W, F140M, F150W, F182M, F162M, F200W, F210M, F250M, F277W, F300M, F335M, F356W, F360M, F410M, F430M, F444W, F460M and F480M. However, not all of the field is covered by every filter, and only the F070W, F090W, F115W, F150W, F200W, F277W, F356, F444W and F460M filters are available for every object, while the coverage by other filters depends on the galaxy's position in the field.

## 2.1. Photometric data

In this paper, we use NIRCam photometry to calculate the UV slopes of high-redshift  $z > 7.5$  galaxies in the CLU and NCF fields. NIRISS observations also exist as deep as those conducted with NIRCam, but we chose not to include them as their filters coverage overlaps with that of NIRCam and would have been redundant. We use photometry measured within a  $0.3''$  circular aperture ( $0.32''$  for the UNCOVER sample) due to the relatively small angular size of most high-redshift sources we're interested in.

For the CANUCS cluster fields, the CLU pointings were mainly observed through all the broad-band filters and the four redder medium-band filters, while all of the NCF pointings were observed through medium- and broad-band filters (refer to Table 1). With the exception of MACS1149 NCF pointing, which is

**Table 1.** Exposure time for the NIRCam filters (in ks) in the surveys used

Filter	CLU+ Bullet	NCF (HFF)	NCF (others)	UNCOVER
F070W	-	10.3	-	8.3
F090W	6.4	10.3	10.3	16.6
F115W	6.4	10.3	10.3	21.6
F140M	-	5.7	5.7	8.3
F150W	6.4	10.3	10.3	21.6
F162M	-	5.7*	5.7	8.3
F182M	-	10.3	10.3	8.3
F200W	6.4	10	-	13.3
F210M	-	10.3	10.3	8.3
F250M	-	5.7*	5.7	8.3
F277M	6.4	10.3	10.3	13.3
F300M	-	5.7	5.7	8.3
F335M	-	10.3	10.3	8.3
F356W	6.4	10	-	13.3
F360M	9.3†	10.3	10.3	8.3
F410M	6.4	10.3	10.3	13.3
F430M	9.3†	10	-	8.3
F444W	6.4	10.3	10.3	16.6
F460M	9.3†	10	-	8.3
F480M	9.3†	10	-	8.3

**Notes.** List of all NIRCam filters used in this work and which pointings use which filter, with their respective exposure time in *ks*. CLU and NCF refer to the main and the flanking position of NIRCam in the fields observed by CANUCS. HFF refers to the Hubble Frontier Field cluster fields: Abell 370, MACS1149 and MACS0416. For details about the limiting magnitude in each pointing, refer to [Sarrouh et al. 2026](#); [Bezanson et al. 2024](#); [Suess et al. 2024](#)

\* denotes a filter missing from MACS1149 NCF pointing.

† Only for CANUCS cluster fields.

missing observations in the F162M and F250M filters. The full description of the NIRCam imaging and its processing can be found in the CANUCS Data Release 1 paper by [Sarrouh et al. \(2026\)](#).

Additionally, HST photometry from observations with the Advanced Camera for Surveys (ACS) – or the Wide Field Camera 3 (WFC3) for the NCF pointing of MACS0417 and MACS1423 – was included to aid in the selection and visual inspection of the sample. The filters included are F435W, F606W, and F814W (F438W and F606W for fields observed with WFC3).

For the Bullet Cluster field we have NIRCam photometry in most broad-band filters and in the F410M medium-band filter.

For Abell 2744, the GLASS, UNCOVER, and MEGASCIENCE surveys provided observations in the full suite of medium- and broad-band filters across most of the field.

## 2.2. Spectroscopic data

For selected objects in the CLU pointings of CANUCS fields, in the Bullet cluster field, and in Abell 2744, we also have NIRSpec low-resolution Prism observations with the MSA, with a typical exposure time of  $\sim 2900$  s. The raw data was processed with a combination of the standard STScI pipeline and the MSAEXP package ([Brammer 2022](#)) including path-loss correction calibrations, in order to obtain 2D spectrum for each source, and 1D spectra were obtained following [Horne \(1986\)](#). A full descrip-

tion of the spectroscopy processing is given in Desprez et al. (2024) and Sarrouh et al. (2026). For Abell 2744 we use the spectral data from Price et al. (2025), available at the DAWN JWST Archive.

### 3. Methodology

#### 3.1. Sample selection

In order to put together a reliable high-redshift sample we obtained a photometric estimate of redshift with the EAzY SED-fitting code (Brammer et al. 2008) for all of the objects in the fields, using updated models accounting for Intergalactic Medium (IGM) and Circumgalactic Medium (CGM) absorption as described in Asada et al. (2025).

A list of high-redshift candidate objects was obtained by applying these criteria, following the same selection procedure as in Willott et al. (2024):

- $S/N < 2$  for the F090W filter
- $S/N > 8$  for the F277W filter
- $z_{EAzY,ML} > 7.5$
- $z_{EAzY,16\%} > 6$

where  $z_{EAzY,ML}$  and  $z_{EAzY,16\%}$  are respectively the maximum-likelihood value and 16th-percentile of the probability density function (PDF) for the redshift parameter in the EAzY SED-fitting procedure. The first criterion ensures that our objects are undetected blueward of Ly- $\alpha$  if they are at  $z > 7.5$ . The F277W criterion constrains our sample to well-detected objects, to avoid objects with poorly determined photometry. The latter criterion is included to avoid possible interlopers with poorly constrained redshift.

The selected objects are then inspected visually, to ensure non-detection in all filters bluer than where each object's Ly- $\alpha$  lies, including the HST filters, and to avoid possible interlopers, spurious objects or image glitches that might have passed the automatic selection. (See Figure 1 for an example of an object in the CLU pointing, with both NIRCam broad-band photometry and NIRSpec Prism spectrum available).

A total of 378 objects were included in our final high-redshift selection. Of these, 212 are part of the five main CANUCS clusters, 36 are in the Bullet cluster, and 130 are from the UNCOVER survey, which has a survey area  $\sim 3$  times larger than each of the 10 individual CANUCS pointing. Of the objects in the CANUCS clusters, 36 also have NIRSpec observations, and for 24 of those the spectra could be used to compute  $\beta$ . The  $M_{UV}$  of two CANUCS cannot be obtained due to missing photometry in a key filter, and two further objects are too faint to compute their  $r_e$ .

We also carried out a comparison between the CANUCS objects found in this work and the objects found using the same criteria in Willott et al. (2024). 57 new objects were included and 54 were left out in our work. This can be explained with having used a new version of the CANUCS photometric catalog after followup observations and updates in the data-processing pipeline: 14 objects in the newer catalog were not present at all in the older version of the catalog, while 13 objects in the older catalog are not included altogether in the newer version. In both cases, this is due to a combination of factors, such as an object being considered part of a larger nearby object in either of the two versions of the catalog.

In other cases, updated photometry processing resulted in slightly different S/N in the F090W and F277W filters for borderline cases, and both additional filters and updated galaxy templates for fitting their spectral energy distribution (SED) resulted

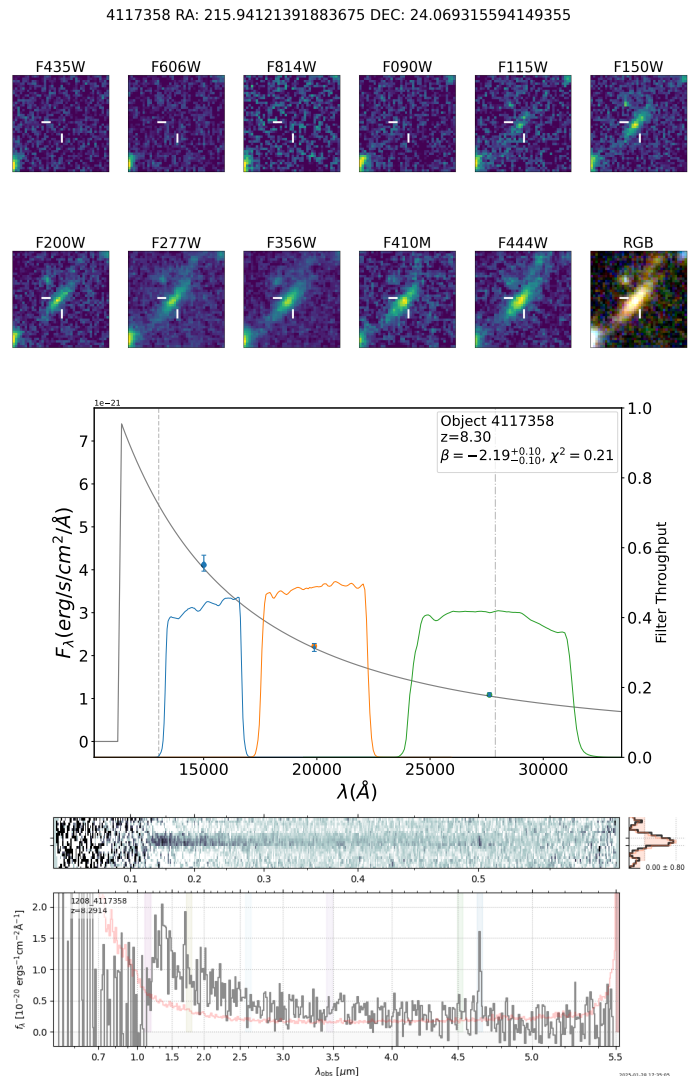


**Fig. 1.** Top panel: NIRCam and ACS images of an example object (CANUCS ID 4117358) in the MACS1423 cluster in the CLU pointing, in all of the filters available for this pointing.

Middle: NIRCam photometry overlaid with the throughput of each NIRCam filter, with the fitted  $\beta$  slope in yellow. The JWST filters' throughput functions are also overlaid in different colours. Vertical dashed (dotted) lines represent the lower (upper) limit for the filters to be used. A hard limit for the lower wavelength threshold, and a soft limit, only limiting the filter's pivot wavelength, for the upper threshold, were applied; in this case, the F150W, F200W and F277W filters were used to fit the UV slope.

Bottom panel: 2D and 1D spectrum for the same object. In the 1D spectrum, the gray line represents the signal, while the red line represents the noise at each wavelength of the spectrum.

in different values for  $z_{ML}$  and  $z_{16\%}$ , and a different set of objects to be sampled.

#### 3.2. Spectroscopic sample

For selected objects of our final photometric sample in the 5 CANUCS fields in the CLU pointing and the Bullet Cluster field, NIRSpec observations are available. For these objects, the spectroscopic redshift  $z_{spec}$  was used in place of  $z_{EAzY,ML}$  when identifying  $z > 7.5$  galaxies, and the criterion  $z_{EAzY,16\%} > 6.0$  was ignored altogether, as the spectroscopic redshift is accurate enough not to require a  $p(z)$  cut. While a wholesale comparison

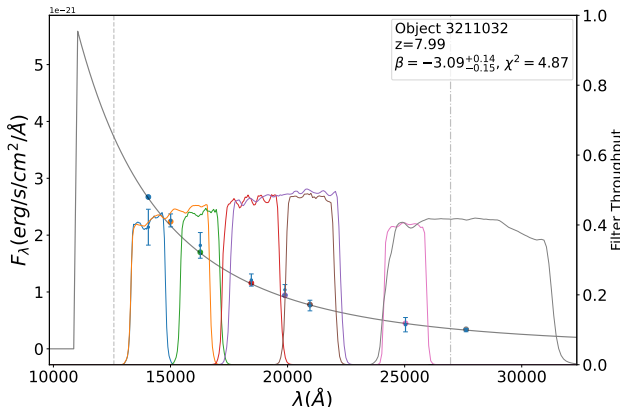


**Fig. 2.** Example of a galaxy at  $z = 7.87$  from the NCF pointing of the MACS0416 field, whose  $\beta$  was calculated from 8 NIRCam filters: F140M, F150W, F162M, F182M, F200W, F210M, and F250M

between spectroscopic and photometric redshift was not carried out for this work, the following resulted: of the 44 targets with spectra with a confirmed  $z_{spec} > 7.5$ , 37 are included in our final high redshift sample. The remaining 7 have no photometry due to being considered part of wider objects. We decided not to include them as we would lack the NIRCam photometry with which to carry out a photometric correction in order to compute their spectral UV slope. Only 24 of these spectra have a spectrum with high enough signal-to-noise ratio (SNR>1.5) in the wavelength range for measuring their UV slope. For two of the objects with  $z_{spec}$ , their  $z_{phot}$  alone would have excluded them from the final sample. This suggests that our final sample could be missing 2 objects for every 35 photometrically-selected ones, or  $\sim 6\%$ ; the rest of our sample (175 objects only selected from photometry) would then potentially lack  $\sim 10$  objects close to the redshift threshold of  $z = 7.5$ .

For the Bullet Cluster and Abell 2744 samples there are respectively 6 and 15 objects with spectroscopy, giving us a total of 45 spectra across all fields.

### 3.3. Measuring UV slopes

There are different methods of measuring the UV slope of a galaxy. One approach is to fit the emission line-free Calzetti et al. (1994) windows with the galaxy's SED obtained from photometric fits, for example using the EAzY code. This however would prevent us from finding extremely blue slopes, as the SED templates do not include the ones with  $\beta < -3.0$ . We decided to rely on a direct power-law fit ( $f_\lambda \propto \lambda^\beta$ ) of the available medium- and wide-band photometry. E.g., Morales et al. (2025) argues in favour of using a direct fit of the photometry for calculating the UV slope, as it recovers the  $\beta$  value found from spectroscopy more accurately than other methods such as SED fitting or single-colour fitting.

#### 3.3.1. Photometric UV slopes

For each object, we picked the JWST filters with rest-frame wavelengths (at a throughput of more than half its maximum) longer than 1400Å, in order to avoid any possible contamination from the Ly- $\alpha$  line, the Ly- $\alpha$  damping wing, and the contribution of two-photon emission in the nebular continuum (Cameron

et al. 2024), which has a peak at around 1340Å. We use photometric redshifts  $z_{phot}$  obtained from EAzY or, where available, its spectroscopic redshift  $z_{spec}$ .

For each object's long-wavelength boundary, we used a softer threshold, by taking filters with pivot wavelength lower than 3200Å, following the method used in Bolamperti et al. (2023). These thresholds leave 2-3 filters, depending on each object's redshift, for the measurement of the UV slope for galaxies in the CLU pointings of NIRCam, where only wide-band filters are available, but up to 8 wide- and medium-band filters in the NCF pointings (e.g. Fig. 2 for a galaxy with  $\beta$  computed from 8 NIRCam filters). We estimated the UV slope of each galaxy with a Markov-chain Monte Carlo (MCMC) fit that convolves the model UV slope  $F_\lambda = A \cdot \lambda^\beta$  with each filter's response function and compares the forward-modeled photometry with that measured in each filter, with  $A$  and  $\beta$  as the free parameters to constrain. We took the median, 16% and 84% of each fit's posterior distribution as the central value, lower, and upper confidence levels respectively.

#### 3.3.2. Spectroscopic UV slopes

Our spectroscopic sample consists of 45 sources across all fields: 24 in the CANUCS fields, 6 in the Bullet Cluster field, and 15 in Abell 2477.

We first adjusted each of the 45 spectra to each object's photometry: we obtained the Spectrum-to-Flux Ratio by convolving the spectrum with each NIRCam filter's throughput function and comparing it with the measured NIRCam photometry; we fitted a 2nd degree Chebyshev polynomial to the Spectrum-to-Flux ratio points at each filter's pivot wavelength; finally we corrected the spectrum with this polynomial, so that the convolution of this corrected spectrum with the NIRCam filters would be equal to the photometry measured in each filter.

We finally estimated the spectroscopic UV-continuum slope index  $\beta_{spec}$  using their photometry-corrected spectrum by fitting a power-law through the Calzetti UV-continuum windows, to avoid contamination from emission lines and dust absorption.

We subsequently carried out a comparison between the photometric ( $\beta_{phot}$ ) and  $\beta_{spec}$  for these objects, finding an average value  $\Delta\beta = \beta_{phot} - \beta_{spec} = -0.2 \pm 0.4$  (see Figure 3), showing that on average the values for the UV slope calculated from photometry are consistent with spectroscopy.

### 3.4. UV magnitudes

We estimate the absolute UV magnitude  $M_{UV}$  for each galaxy in all cluster fields using the brightness  $F_\nu$  in the NIRCam filter closest to 1500Å which does not include the Ly- $\alpha$  line. The brightness is corrected with each object's estimated lensing magnification  $\mu$ . We then rescale the magnitude found with such filter to 1500Å with the following formula:

$$M_{1500\text{Å}} = M_{\lambda_{\text{pivot}}} - 2.5(\beta - 2)\log_{10}\left(\frac{1500\text{Å}}{\lambda_{\text{pivot}}}\right)$$

Where  $\lambda_{\text{pivot}}$  is the pivot wavelength of the filter used.

The best-fit values of  $\mu$  were obtained from the lensing model for MACS0416 (Rihtaršič et al. 2025), Abell 370 (Gledhill et al. 2024), MACS0417 (Desprez et al. *in prep.*), and MACS1423 (Desprez et al. *in prep.*), and MACS1149 and the Bullet Cluster (Rihtaršič et al. 2026). The lensing models are also available in the CANUCS Data Release 1 (DR1) and described in Sarrouh

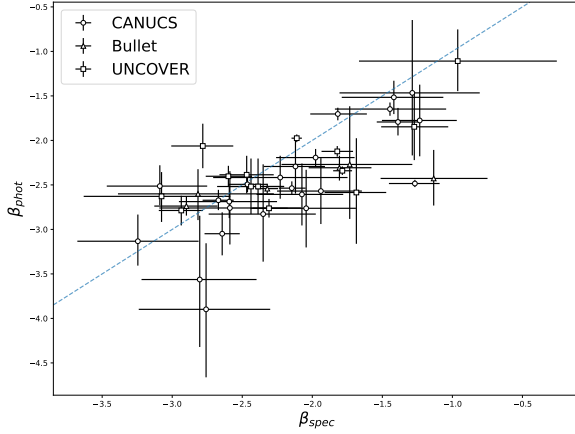


**Fig. 3.** *Main:* Comparison between photometric and spectroscopic values for the UV slope's  $\beta$  index, for 14 galaxies in our sample; the dashed blue line represents  $\beta_{phot} = \beta_{spec}$ .

et al. (2026). The lensing model for Abell 2744 is described in Furtak et al. (2023) and Price et al. (2025).

## 4. Results

For our whole sample, we have an average value of  $\beta = -2.3 \pm 0.4$ , weighting each value of  $\beta$  with its inverse variance. The values range from -4.0 to -0.5 (see Fig. 4). We also find our objects to be at an average redshift of  $z = 8.5 \pm 1.1$  and to have an average  $M_{UV} = -18.9 \pm 1.2$ .

In Figure 4, we show the trend between the UV slope and redshift of all galaxies in our sample. The pale blue points represent the objects for which we have photometric values of  $\beta$ , while the yellow data points represent spectroscopic values. Circle, triangle and square-shaper points refer to objects in the CANUCS fields, Bullet Cluster, and Abell 2744 respectively. Fitting the whole sample we find no significant trend between  $\beta$  and redshift:  $d\beta/dz = 0.02^{+0.02}_{-0.03}$ .

In Figure 5 we show the relationship between  $\beta$  and  $M_{UV}$ , colour-coded as in Figure 4. We find  $d\beta/dM_{UV} = -0.06^{+0.03}_{-0.02}$  across our whole sample, suggesting a very weak trend of UV slope with galaxy brightness, at least compared to previous literature results.

In Figure 6) we bin the data to compare with existing literature, and we find similar results. However, due to the large scatter in our data and the limited statistics, our results are very sensitive to the choice of binning.

### 4.1. LyC escape fraction

In recent years, several works have tried to estimate the escape fraction of LyC photons in high-redshift galaxies, either from relations calibrated at low-redshift (Chisholm et al. 2022; Lin et al. 2024), or using predictions from cosmological simulations (i.e. Saxena et al. 2024; Choustikov et al. 2024). It should be noted that some models do not rely on low-redshift calibration and instead use SED fitting of spectral features to model the effect of LyC leakage on emission lines and UV slope (see for example Giovinazzo et al. 2025). Here, we will use the model presented in Mascia et al. (2024), which was calibrated on the low-redshift galaxy sample of Flury et al. (2022). It makes use of the half-

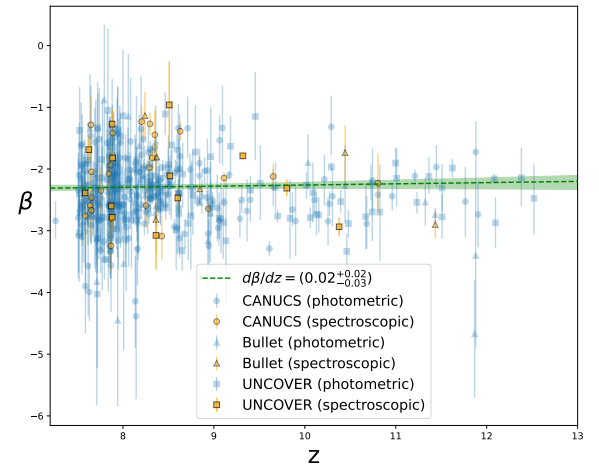


**Fig. 4.**  $\beta - z$  diagram for our high-redshift sample. Objects for which only photometric estimates of  $\beta$  are available are plotted in blue, and spectral estimates of  $\beta$  are in orange; for objects that have both we only plot spectral estimates. A linear fit of the trend and its shaded 1- $\sigma$  confidence level, obtained via a bootstrap method, is also represented.

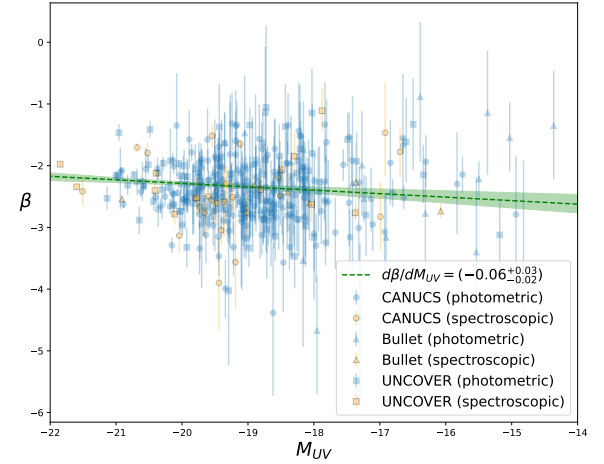


**Fig. 5.**  $\beta - M_{UV}$  diagram, color code is the same as in Figure 4. The green dashed line represents the relationship found between  $\beta$  and  $M_{UV}$  for the whole sample, with the green shaded region representing a 1- $\sigma$  confidence band. Plot points representing galaxies in the UNCOVER sample are reported with blue diamonds, as we calculated their  $M_{UV}$  with a different process with respect to the CANUCS clusters.

light radius  $r_e$ , the equivalent width of  $H\beta$   $EW_0(H\beta)$ , and the  $\beta$  index of the UV slope of a galaxy to predict its LyC escape fraction:

$$\log_{10} f_{esc} = A + B \cdot EW(H\beta) + C \cdot r_e + D \cdot \beta$$

Where the values of the coefficients A, B, C, and D are those reported in Mascia et al. (2024).

In our sample, it was possible to obtain measurements for all three properties for 14 galaxies in total, as  $H\beta$  measurements require NIRSpec data. The size measurements were obtained by Judež et al. (*in prep.*) with the same method as in Willott et al. (2025): using a forward modeling procedure of galaxy shapes

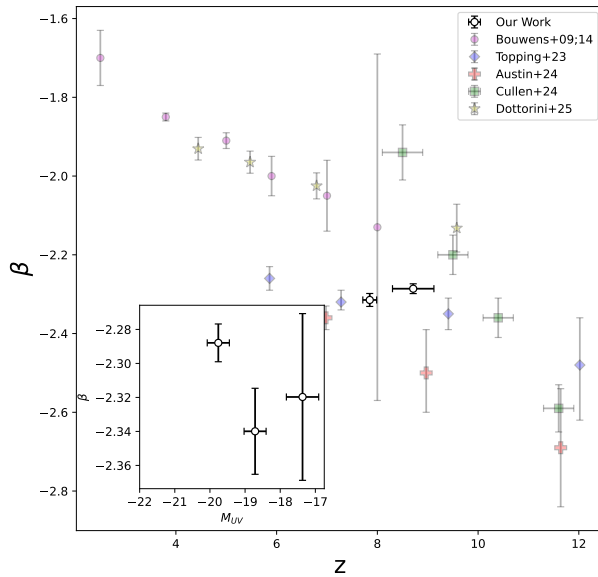


**Fig. 6.**  $\beta$ - $z$  diagram (inset:  $\beta$  -  $M_{UV}$  diagram) for our sample in redshift ( $M_{UV}$ ) bins. White circles - in the vertical direction, the weighted mean of  $\beta$  in each bin, with the standard deviation of each subsample as its error bar; in the horizontal direction: the median and upper and lower limit of the redshift ( $M_{UV}$ ) in each bin. Coloured data points - values from previous works: purple circles from Bouwens et al. (2014), blue diamonds from Topping et al. (2023), red crosses from Austin et al. (2024), green squares from Cullen et al. (2024), and yellow stars from Dottorini et al. (2024).

through the strong lensing field using the LENSTRUCTION software (Yang et al. 2020; Birrer et al. 2015; Birrer & Amara 2018). For one of these objects, the extrapolation yields a non-physical value of  $f_{esc} > 1$ , because of an extremely high  $H\beta$  equivalent width of  $(886 \pm 41)\text{\AA}$ . That object was not included in the final  $f_{esc}$  sample, leaving us with 14 galaxies.

The confidence intervals were obtained with a MC method by resampling the value of each parameter and coefficient 1000 times within its distribution. The detailed results are reported in Table 2. We find an average escape fraction of  $0.26 \pm 0.22$  across our sample, slightly higher than the averages found in Mascia et al. (2024) for objects at  $< z > = 8$  but with a much greater dispersion.

## 5. Discussion

### 5.1. UV slope trends

The absence of a trend of  $\beta$  with redshift is in contrast with previous studies at lower redshifts (e.g. Bouwens et al. 2014; Bolamperti et al. 2023), which all seem to find a negative trend with bluer slopes at higher redshifts. However, more recent studies made possible by JWST include galaxies at redshifts  $z > 7$ , and also to find a flattening of this relation at the highest redshifts (e.g. Saxena et al. 2024; Roberts-Borsani et al. 2025). Our results seem to support these latest studies, and a confirm flattening of the overall slope in the UV at the higher redshifts. The flattening of this relation may indicate that a wider portion of galaxies at high- $z$  have their UV emission dominated by the nebular continuum with an intrinsic  $\beta \sim -2.3$ , and that could explain why

we don't see a continuing of the trend at lower redshift. On the other hand, it's important also to note the limited statistics of our sample especially at  $z > 9$  and the fact that the redshift ranges  $7.5 < z < 9$  and  $9 < z < 12$  only span 150 to 200 Myr each, which may not be enough to register a change in the overall UV slope.

We also find a very weak trend between  $\beta$  and  $M_{UV}$ , with lower  $\beta$  for fainter galaxies. This is in contrast with studies at lower redshift which usually find that fainter and less massive galaxies have bluer slopes Bouwens et al. (2010, 2014); Topping et al. (2023). In our work we find instead a weak relation, in agreement with what is found by Saxena et al. (2024), where for a subsample at  $z > 8$  they find a similar trend. This seems to give credit to the model in which both high- and low-mass galaxies achieve similarly steep slopes during the first starforming episodes, but more massive and brighter galaxies accumulate dust more rapidly, leading to redder UV slopes at lower redshift. It should be noted that the trend between UV slope and magnitude is however affected by a large scatter in the galaxy population, compounded by large uncertainties in lensing model magnifications, which make this relation less robust.

### 5.1.1. Differences photometric and spectroscopic measurement of $\beta$

We find consistent measurements between photometric and spectroscopic UV slopes in our sample, with  $< \Delta \beta > = 0.2 \pm 0.4$ . However there are a handful of objects for which the offset is significant. For a few of those, the discrepancy is driven by the different regions of a galaxy captured by spectroscopic and photometric procedures. E.g. for the Firefly Sparkle galaxy (Mowla et al. 2024) the spectrum has been mainly obtained from the central clump, while the  $0\farcs3$  aperture photometry also captures the light from two adjacent, much bluer clumps, leading to bluer slopes being measured from the photometry. In other cases, the discrepancy is due to the number of photometric filters used to measure the UV slope and sampling part of the spectrum redward of the Calzetti et al. (1994) windows. This could lead to a discrepancy especially for the galaxies in the CLU field, for which we have fewer filters available, in several cases only 2 per galaxy, in order to measure the slope. This issue is alleviated in the NCF fields, where medium-band filters are available in the same wavelength range in addition to the broadband filters.

### 5.2. Extrapolation of LyC $f_{esc}$

Finally, we extrapolated the values of the LyC escape fraction  $f_{esc}$  for a subsample of 14 galaxies observed with NIRSpec and for which we have emission line measurements (see Table 2). We found an average escape fraction of  $0.26 \pm 0.22$  across the subsample, a moderately high value with respect with the  $\sim 10\%$  that would be required to ionize most of the IGM by  $z \sim 6$  (Finkelstein et al. 2019), but the wide scatter puts it in agreement with values found by Mascia et al. (2024). These values should be taken with a grain of salt, as the date used to calibrate the relation in Mascia et al. (2024) was done on a sample of galaxies at low redshift (Flury et al. 2022) where the direct measurement of  $f_{esc}$  is possible, and the extrapolation we did assumes that the same calibration would hold true at the EoR. Giovinazzo et al. (2025) argue that relations already doesn't hold anymore between  $z \sim 0.3$  and  $z \sim 3$ , as the change in the galactic environment can affect these relations, as at high redshift the higher rate of galaxy mergers and other galaxy interactions would affect the

**Table 2.** Physical properties of the 14 objects in our  $f_{esc}$  sample

CANUCS ID	RA	DEC	$EW_0(H\beta)$	$r_e$ (kpc)	$\beta$	$f_{esc}$ (LyC)
1106089	64.376136	-11.908745	$33 \pm 9$	$0.02^{+0.01}_{-0.01}$	$-3.0 \pm 0.3$	$0.20^{+0.30}_{-0.07}$
2110006	39.975840	-1.587273	$190 \pm 40$	$0.110^{+0.005}_{-0.005}$	$-2.6 \pm 0.3$	$0.30^{+0.50}_{-0.10}$
2120090	39.966109	-1.594787	$440 \pm 70$	$0.045^{+0.012}_{-0.019}$	$-1.8 \pm 0.5$	$0.8^{+2.3}_{-0.6}$
3107165	64.039230	-24.093198	$170 \pm 30$	$0.54^{+0.01}_{-0.01}$	$-1.7 \pm 0.1$	$0.05^{+0.03}_{-0.01}$
3113053	64.043179	-24.057928	$70 \pm 20$	$0.034^{+0.006}_{-0.003}$	$-3.2 \pm 0.4$	$0.30^{+0.70}_{-0.10}$
3114538	64.039317	-24.045717	$10 \pm 10$	$0.16^{+0.02}_{-0.02}$	$-2.4 \pm 0.3$	$0.085^{+0.092}_{-0.027}$
3117269	64.048130	-24.081449	$110 \pm 20$	$0.269^{+0.01}_{-0.009}$	$-1.6 \pm 0.1$	$0.061^{+0.022}_{-0.019}$
4100225	215.942388	24.069652	$210 \pm 140$	$0.13^{+0.01}_{-0.009}$	$-2.5 \pm 0.1$	$0.38^{+0.70}_{-0.09}$
4117337	215.944441	24.068745	$150 \pm 180$	$0.022^{+0.004}_{-0.003}$	$-1.7 \pm 0.2$	$0.12^{+0.27}_{-0.033}$
4117358	215.941214	24.069316	$20 \pm 180$	$0.147^{+0.007}_{-0.007}$	$-2.2 \pm 0.1$	$0.071^{+0.14}_{-0.017}$
5101296	177.379426	22.345013	$330 \pm 10$	$0.056^{+0.031}_{-0.025}$	$-2.3 \pm 0.5$	$0.63^{+0.94}_{-0.16}$
5104911	177.359469	22.375533	$100 \pm 100$	$0.045^{+0.024}_{-0.019}$	$-2.0 \pm 0.3$	$0.13^{+0.35}_{-0.036}$
5110240	177.389947	22.412704	$220 \pm 80$	$0.087^{+0.009}_{-0.007}$	$-2.5 \pm 0.2$	$0.36^{+0.53}_{-0.10}$
5112687	177.390930	22.349767	$90 \pm 80$	$0.029^{+0.015}_{-0.013}$	$-1.8 \pm 0.3$	$0.098^{+0.21}_{-0.029}$

star formation process and the creation or obscuration of LyC leakage channels.

## 6. Summary and Conclusions

We use photometric and spectroscopic data from JWST NIRCam and NIRSpec instrument gathered by 6 surveys across 7 strong lensing fields: CANUCS for the clusters MACS0417, MACS0416, Abell370, MACS1149 and MACS1423, Technicolor and JUMPS for MACS0416, Abell370, and MACS1149; *Silver Bullet for Dark Matter* for the Bullet Cluster; GLASS, UNCOVER and MEGASCIENCE for Abell 2477. We analyse the UV slopes ( $\beta$ ) in a sample of 378 galaxies at  $7.5 < z < 12.5$ . Thanks to the high magnification provided by the 7 cluster fields targeted by these surveys, we are able to recover galaxies down to a magnitude of  $M_{UV} \lesssim -16$  in the main cluster pointing. We are also able to more robustly estimate values of  $\beta$  in the NCF fields thanks to the numerous medium-band filters employed by CANUCS, TECHNICOLOR and UNCOVER. The combination of these two factors, the very deep data in the CLU pointing and the very accurate data in the NCF, allows for a powerful analysis of the trends of  $\beta$ . We also carry out a comparison with the spectroscopic  $\beta$  slopes measured for 30 of the galaxies, after correcting the spectra with photometry, and find no statistically significant offset of bluer slopes with photometry with respect to spectroscopy. We find however few individual objects with significant offsets, mainly due to different parts of each galaxy being probed by NIRCam and NIRSpec, while the effect of possible slit-losses on the UV slope when observing with the NIRSpec instrument has already been addressed by correcting the spectrum with the photometry itself. We find that:

1. We find no significant trend between  $\beta$  and redshift, with  $d\beta/dz = 0.00^{+0.02}_{-0.03}$  over the range  $7.5 < z < 12.5$ , consistent with a flattening of the relation past  $z > 7$  found in recent works. This underlines the similarity in average galaxy properties between  $\sim 300$  and  $\sim 600$  Myr after the Big Bang, with most of the scatter due the variance in galaxy properties, and possibly due in part to a strong contribution from the nebular continuum and an absence of dust which would redden the slopes.
2. We find a weak trend between  $\beta$  and  $M_{UV}$   $d\beta/dM_{UV} = -0.06 \pm 0.03$  over the whole UV magnitude range of  $-22 < M_{UV} < -16$ , also consistent with recent results at high-redshift (Saxena et al. 2024, Austin et al. 2024). This could be pointing to a lack of dust, or at least to an absence of correlation between dust and SFR for galaxies in the interval  $7.5 < z < 12.5$ , with more massive galaxies not having had yet enough time to build up a dust reservoir with respect to less massive ones.
3. Using a model from Mascia et al. (2024) that uses the UV slope, H $\beta$  equivalent width and galaxy sizes, we extrapolate LyC escape fractions for 14 galaxies in our sample, and find an average  $\langle f_{esc} \rangle = 0.26 \pm 0.22$  between redshifts of  $\sim 8$  and  $\sim 11$ , in line with previous values found in literature. This is a relatively high value of  $f_{esc}$  with respect to what predicted to obtain neutral IGM at  $z \sim 6$ . The wide scatter in the subsample and the extrapolation obtained from low- $z$  galaxies lead us to take this result with a grain of salt

*Acknowledgements.* GF, MB, JJ, GR, NM, AH, and VM acknowledge support from the ERC Grant FIRSTLIGHT # 101053208, Slovenian national research agency ARIS through grants N1-0238 and P1-0188, and ESA PRODEX Experiment Arrangements No. 4000146646 and 4000149972. This research was also enabled by grant 18JWST-GTO1 from the Canadian Space Agency and funding

from the Natural Sciences and Engineering Research Council of Canada. This research used the Canadian Advanced Network For Astronomy Research (CAN-FAR) operated in partnership by the Canadian Astronomy Data Centre and The Digital Research Alliance of Canada with support from the National Research Council of Canada the Canadian Space Agency, CANARIE and the Canadian Foundation for Innovation. The data were obtained from the Mikulski Archive for Space Telescopes at the Space Telescope Science Institute, which is operated by the Association of Universities for Research in Astronomy, Inc., under NASA contract NAS 5-03127 for JWST. Support for program #4598 was provided by NASA through a grant from the Space Telescope Science Institute, which is operated by the Association of Universities for Research in Astronomy, Inc., under NASA contract NAS 5-03127.

## References

Aghanim, N., Akrami, Y., Ashdown, M., et al. 2020, *Astronomy & Astrophysics*, 641, A6 [2](#)

Asada, Y., Desprez, G., Willott, C. J., et al. 2025, *The Astrophysical Journal*, 983, L2, publisher: IOP ADS Bibcode: 2025ApJ...983L...2A [2](#), [4](#)

Austin, D., Conselice, C. J., Adams, N. J., et al. 2024, EPOCHS III: Unbiased UV continuum slopes at 6.5, publication Title: arXiv e-prints ADS Bibcode: 2024arXiv240410751A [2](#), [7](#), [8](#)

Bagley, M. B., Pirzkal, N., Finkelstein, S. L., et al. 2024, *The Astrophysical Journal*, 965, L6, aDS Bibcode: 2024ApJ...965L...6B [2](#)

Bezanson, R., Labbe, I., Whitaker, K. E., et al. 2024, *The Astrophysical Journal*, 974, 92, publisher: IOP ADS Bibcode: 2024ApJ...974...92B [2](#), [3](#)

Birrer, S. & Amara, A. 2018, Lenstronomy: multi-purpose gravitational lens modelling software package, arXiv:1803.09746 [astro-ph] version: 1 [7](#)

Birrer, S., Amara, A., & Refregier, A. 2015, *The Astrophysical Journal*, 813, 102, aDS Bibcode: 2015ApJ...813..102B [7](#)

Bolamperti, A., Zanella, A., Meštrić, U., et al. 2023, UV-continuum  $\beta$  slopes of individual  $z \sim 2 - 6$  clumps and their evolution, arXiv:2310.04498 [astro-ph] [2](#), [5](#), [7](#)

Bouwens, R. J., Illingworth, G. D., Oesch, P. A., et al. 2014, *The Astrophysical Journal*, 793, 115, publisher: The American Astronomical Society [2](#), [7](#)

Bouwens, R. J., Illingworth, G. D., Oesch, P. A., et al. 2010, *The Astrophysical Journal*, 708, L69, publisher: IOP ADS Bibcode: 2010ApJ...708L..69B [2](#), [7](#)

Brammer, G. 2022, gbrammer/msaexp: Full working version with 2d drizzling and extraction [3](#)

Brammer, G. B., Van Dokkum, P. G., & Coppi, P. 2008, *The Astrophysical Journal*, 686, 1503 [4](#)

Calzetti, D., Kinney, A. L., & Storchi-Bergmann, T. 1994, *The Astrophysical Journal*, 429, 582 [2](#), [5](#), [7](#)

Cameron, A. J., Katz, H., Witten, C., et al. 2024, *Monthly Notices of the Royal Astronomical Society*, 534, 523, aDS Bibcode: 2024MNRAS.534..523C [5](#)

Chisholm, J., Saldana-Lopez, A., Flury, S., et al. 2022, *Monthly Notices of the Royal Astronomical Society*, 517, 5104, publisher: OUP ADS Bibcode: 2022MNRAS.517.5104C [2](#), [6](#)

Choustikov, N., Katz, H., Saxena, A., et al. 2024, *Monthly Notices of the Royal Astronomical Society*, 529, 3751, aDS Bibcode: 2024MNRAS.529.3751C [2](#), [6](#)

Cullen, F., McLeod, D. J., McLure, R. J., et al. 2024, *Monthly Notices of the Royal Astronomical Society*, 531, 997, publisher: OUP ADS Bibcode: 2024MNRAS.531..997C [2](#), [7](#)

Desprez, G., Martis, N. S., Asada, Y., et al. 2024, *Monthly Notices of the Royal Astronomical Society*, 530, 2935, publisher: OUP ADS Bibcode: 2024MNRAS.530.2935D [4](#)

Dottorini, D., Calabro, A., Pentericci, L., et al. 2024, Evolution of the UV slope of galaxies at cosmic morning ( $z > 4$ ): the properties of extremely blue galaxies, publication Title: arXiv e-prints ADS Bibcode: 2024arXiv241201623D [2](#), [7](#)

Eisenstein, D. J., Willott, C., Alberts, S., et al. 2023, Overview of the JWST Advanced Deep Extragalactic Survey (JADES), arXiv:2306.02465 [astro-ph] [2](#)

Finkelstein, S. L., Bagley, M. B., Ferguson, H. C., et al. 2023, *The Astrophysical Journal*, 946, L13, publisher: IOP ADS Bibcode: 2023ApJ...946L..13F [2](#)

Finkelstein, S. L., D'Aloisio, A., Paardekooper, J.-P., et al. 2019, *The Astrophysical Journal*, 879, 36, aDS Bibcode: 2019ApJ...879...36F [7](#)

Flury, S. R., Jaskot, A. E., Ferguson, H. C., et al. 2022, *The Astrophysical Journal*, 930, 126, publisher: The American Astronomical Society [2](#), [6](#), [7](#)

Furtak, L. J., Zitrin, A., Weaver, J. R., et al. 2023, *Monthly Notices of the Royal Astronomical Society*, 523, 4568, aDS Bibcode: 2023MNRAS.523.4568F [6](#)

Giovinazzo, E., Oesch, P. A., Weibel, A., et al. 2025, Breaking Through the Cosmic Fog: JWST/NIRSpec Constraints on Ionizing Photon Escape in Reionization-Era Galaxies, aDS Bibcode: 2025arXiv250701096G [6](#), [7](#)

Gledhill, R., Strait, V., Desprez, G., et al. 2024, CANUCS: An Updated Mass and Magnification Model of Abell 370 with JWST, arXiv:2403.07062 [astro-ph] [5](#)

Horne, K. 1986, *Publications of the Astronomical Society of the Pacific*, 98, 609, publisher: IOP Publishing [3](#)

Lin, Y.-H., Scarlata, C., Williams, H., et al. 2024, *Monthly Notices of the Royal Astronomical Society*, 527, 4173, aDS Bibcode: 2024MNRAS.527.4173L [6](#)

Mascia, S., Pentericci, L., Calabro, A., et al. 2024, *Astronomy and Astrophysics*, 685, A3, publisher: EDP ADS Bibcode: 2024A&A...685A...3M [2](#), [6](#), [7](#), [8](#)

Mascia, S., Pentericci, L., Calabro, A., et al. 2023, *Astronomy and Astrophysics*, 672, A155, aDS Bibcode: 2023A&A...672A.155M [2](#)

Morales, A. M., Finkelstein, S. L., Haro, P. A., et al. 2025, Testing Photometric Techniques for Measuring the Rest-Frame UV Spectral Slope Against JWST PRISM Spectroscopy, arXiv:2507.03118 [astro-ph] [5](#)

Mowla, L., Iyer, K., Asada, Y., et al. 2024, *Nature*, 636, 332 [7](#)

Price, S. H., Bezanson, R., Labbe, I., et al. 2025, *The Astrophysical Journal*, 982, 51, aDS Bibcode: 2025ApJ...982...51P [4](#), [6](#)

Pérez-González, P. G., Östlin, G., Costantin, L., et al. 2025, *The Astrophysical Journal*, 991, 179, aDS Bibcode: 2025ApJ...991..179P [2](#)

Rihtaršić, G., Bradač, M., Desprez, G., et al. 2026, Mapping dark matter in the Bullet Cluster using JWST imaging and spectroscopy, arXiv:2601.22245 [astro-ph] [2](#), [5](#)

Rihtaršić, G., Bradač, M., Desprez, G., et al. 2025, *Astronomy and Astrophysics*, 696, A15, aDS Bibcode: 2025A&A...696A..15R [5](#)

Roberts-Borsani, G., Oesch, P., Ellis, R., et al. 2025, JWST Spectroscopic Insights Into the Diversity of Galaxies in the First 500 Myr: Short-Lived Snapshots Along a Common Evolutionary Pathway, aDS Bibcode: 2025arXiv250821708R [7](#)

Sarrouh, G. T. E., Asada, Y., Martis, N. S., et al. 2026, *The Astrophysical Journal Supplement Series*, 282, 3, aDS Bibcode: 2026ApJS..282...3S [2](#), [3](#), [4](#), [5](#)

Saxena, A., Cameron, A. J., Katz, H., et al. 2024, Hitting the slopes: A spectroscopic view of UV continuum slopes of galaxies reveals a reddening at  $z > 9.5$ , aDS Bibcode: 2024arXiv241114532S [2](#), [6](#), [7](#), [8](#)

Suess, K. A., Weaver, J. R., Price, S. H., et al. 2024, *The Astrophysical Journal*, 976, 101 [2](#), [3](#)

Topping, M. W., Stark, D. P., Endsley, R., et al. 2023, The UV Continuum Slopes of Early Star-Forming Galaxies in JADES, publication Title: arXiv e-prints ADS Bibcode: 2023arXiv230708835T [2](#), [7](#)

Treu, T., Roberts-Borsani, G., Bradac, M., et al. 2022, *The Astrophysical Journal*, 935, 110 [2](#), [3](#)

Whitler, L., Stark, D. P., Topping, M. W., et al. 2025, *The Astrophysical Journal*, 992, 63, aDS Bibcode: 2025ApJ...992...63W [2](#)

Willott, C. J., Asada, Y., Iyer, K. G., et al. 2025, *The Astrophysical Journal*, 988, 26, aDS Bibcode: 2025ApJ...988...26W [6](#)

Willott, C. J., Desprez, G., Asada, Y., et al. 2024, *The Astrophysical Journal*, 966, 74, publisher: IOP ADS Bibcode: 2024ApJ...966...74W [4](#)

Willott, C. J., Doyon, R., Albert, L., et al. 2022, *Publications of the Astronomical Society of the Pacific*, 134, 025002, publisher: IOP ADS Bibcode: 2022PASP..134b5002W [2](#)

Windhorst, R. A., Cohen, S. H., Jansen, R. A., et al. 2023, *The Astronomical Journal*, 165, 13, aDS Bibcode: 2023AJ....165...13W [2](#)

Yang, L., Birrer, S., & Treu, T. 2020, *Monthly Notices of the Royal Astronomical Society*, 496, 2648, arXiv:2001.07719 [astro-ph] [7](#)

Zackrisson, E., Inoue, A. K., & Jensen, H. 2013, *The Astrophysical Journal*, 777, 39, publisher: IOP ADS Bibcode: 2013ApJ...777...39Z [2](#)